The Astrophysical Journal Letters, 777:L3 (5pp), 2013 November 1 doi:10.1088/2041-8205/777/1/L3

LIMITS ON ALPHA PARTICLE TEMPERATURE ANISOTROPY AND DIFFERENTIAL FLOW FROM KINETIC INSTABILITIES: SOLAR WIND OBSERVATIONS

Sofiane Bourouaine[1], Daniel Verscharen[1], Benjamin D. G. Chandran[1], Bennett A. Maruca[2], and Justin C. Kasper[3]
[1] Space Science Center, University of New Hampshire, Durham, NH 03824, USA; s.bourouaine@unh.edu
[2] Space Science Laboratory, University of California, Berkeley, CA 94720, USA
[3] Harvard-Smithsonian Center for Astrophysics, Cambridge, MA 02138, USA
Received 2013 July 30; accepted 2013 September 16; published 2013 October 9

ABSTRACT

Previous studies have shown that the observed temperature anisotropies of protons and alpha particles in the solar wind are constrained by theoretical thresholds for pressure and anisotropy driven instabilities such as the Alfvén/ion-cyclotron (A/IC) and fast-magnetosonic/whistler (FM/W) instabilities. In this Letter, we use a long period of in situ measurements provided by the *Wind* spacecraft's Faraday cups to investigate the combined constraint on the alpha proton differential flow velocity and the alpha particle temperature anisotropy due to A/IC and FM/W instabilities. We show that the majority of the data are constrained to lie within the region of parameter space in which A/IC and FM/W waves are either stable or have extremely low growth rates. In the minority of observed cases in which the growth rate of the A/IC (FM/W) instability is comparatively large, we find relatively higher values of $T_{\perp\alpha}/T_{\perp p}$ ($T_{\parallel\alpha}/T_{\parallel p}$) when the alpha proton differential flow velocity is small, where $T_{\perp\alpha}$ and $T_{\perp p}$ ($T_{\parallel\alpha}$ and $T_{\parallel p}$) are the perpendicular (parallel) temperatures of alpha particles and protons. We conjecture that this observed feature might arise from preferential alpha particle heating which can drive the alpha particles beyond the instability thresholds.

Key words: instabilities – solar wind – turbulence – waves

Online-only material: color figures

1. INTRODUCTION

In situ spacecraft measurements indicate that solar wind plasma deviates significantly from local thermodynamic equilibrium. Ions exhibit distinct non-thermal kinetic features, such as proton core temperature anisotropy, proton beams, and the preferential heating and acceleration (with respect to the protons) of alpha particles and minor ions (Marsch 2006). All these non-thermal features can be a source of kinetic instabilities, such as the Alfvén/ion-cyclotron (A/IC), mirror mode, fast-magnetosonic/whistler (FM/W), and oblique firehose (FH) instabilities.

During the transit of the ions from the Sun to a heliospheric distance r of 1 AU, the adiabatic expansion of the solar wind tends to drive a temperature anisotropy of the form $T_\parallel > T_\perp$, where $\parallel$ and $\perp$ refer to the directions parallel and perpendicular to the local magnetic field (Chew et al. 1956). On the other hand, ions can be imparted with the opposite sense of temperature anisotropy by heating from either the dissipation of low-frequency turbulence (Dmitruk et al. 2004; Parashar et al. 2009; Bourouaine et al. 2008; Chandran et al. 2010) or resonant cyclotron interactions with high-frequency A/IC waves (Isenberg et al. 2001; Marsch & Tu 2001; Hollweg and Isenberg 2002; Gary et al. 2006). *Wind* measurements at 1 AU reveal that the temperature anisotropy of protons and alpha particles can be a source for A/IC, mirror mode, FM/W, and oblique FH instabilities (Kasper et al. 2002; Hellinger et al. 2006; Bale et al. 2009; Maruca et al. 2012). Also, *Helios* measurements near 0.3 AU show that the velocity distribution functions of the proton core in fast solar wind regions are close to marginal stability for the A/IC instability (Bourouaine et al. 2010).

In situ measurements in the inner heliosphere indicate that alpha particles can be accelerated up to the local Alfvén speed in the proton frame (Marsch et al. 1982; Neugebauer et al. 1994; Bourouaine et al. 2011a, 2011b). However, the differential speed between alpha particles and protons rarely exceeds the local Alfvén speed, because super-Alfvénic alpha particle beams lead to the excitation of A/IC and FM/W waves (Li & Habbal 2000; Gary et al. 2000; Verscharen & Chandran 2013), and the amplified waves can decelerate the alpha particles (Kaghashvili et al. 2004; Lu et al. 2009).

Collisions in the solar wind tend to equilibrate the plasma to a state far below the instability thresholds. Nevertheless, the collisionally regulated plasma can still excite waves if it approaches a threshold for instabilities with sufficiently high growth rates.

Some previous studies have focused on instabilities driven by either an alpha particle temperature anisotropy $R_\alpha = T_{\perp\alpha}/T_{\parallel\alpha} \neq 1$ or a non-zero average alpha particle velocity U_α in the proton rest frame. However, other studies have shown that temperature anisotropy modifies the U_α thresholds of the A/IC and FM/W instabilities, while differential flow modifies the R_α thresholds of these instabilities (Gary 1993; Araneda et al. 2002; Gary et al. 2003; Hellinger et al. 2003; Verscharen et al. 2013). Our goal in this Letter is thus to treat U_α and R_α on an equal footing and, by analyzing data from the *Wind* spacecraft, to determine whether the linear A/IC and FM/W instabilities provide a good explanation for the limits on U_α and R_α that are observed in the solar wind.

2. OBSERVATIONS AND RESULTS

The measurements of ion parameters used in this study were derived from in situ data from the *Wind* spacecraft's Faraday cups (Ogilvie et al. 1995). This instrument produces an ion spectrum (i.e., a distribution of ion speeds projected along various axes) about once every ninety seconds. The bulk

parameters (e.g., density, flow velocity, and temperature) of the protons and alpha particles can be deduced from each spectrum by fitting a model velocity distribution function for each species (Kasper 2002; Kasper et al. 2006). Perpendicular and parallel temperature components can be separated using measurements of the local magnetic field, which are available from *Wind*'s Magnetic Field Investigation (Lepping et al. 1995).

For this study, we use the dataset of ion parameters produced by Maruca (2012, Chapter 4), who processed nearly 4.8 million *Wind* ion spectra (i.e., all spectra from the spacecraft's launch in late 1994 through mid-2010) with a fully-revised fitting code. These revisions dramatically improved the code's analysis of temperature anisotropy and differential flow (especially during periods of significant fluctuations in the background magnetic field) (Maruca & Kasper 2013). Nevertheless, only about 2.1 million of the spectra processed were included in the final dataset due to two sets of selection requirements. First, a spectrum needed to have been measured at a time when *Wind* was well outside the Earth's bow shock (i.e., actually in the solar wind). The spacecraft, especially during the early part of its mission, spent significant amounts of time exploring the Earth's magnetosphere. Second, the fit results had to be of high quality as gauged by reduced-χ^2, uncertainty in the fit parameters, and other metrics. The most frequent cause for this second criterion not being met was low alpha particle signal (from, e.g., low densities or high temperatures).

To study the instabilities resulting from a combination of relative drift and temperature anisotropy of alpha particles, we restrict our data analysis to solar wind intervals in which $3 \leqslant T_\alpha/T_\mathrm{p} \leqslant 5$. The selected interval of T_α/T_p represents the typical range of variation of the ratio alpha-to-proton temperature in weakly collisional solar wind streams (Kasper et al. 2008). Also, our selection is consistent with the theoretical value of $3 \lesssim T_\alpha/T_\mathrm{p} \lesssim 5$ used below to determine the threshold values for the drift–anisotropy instabilities.

Using Kennel & Wong's (1967) expression for the growth rate γ of weakly growing waves, Verscharen et al. (2013) derived approximate analytic expressions for the instability thresholds of A/IC and FM/W waves taking into account both the alpha proton drift and alpha particle temperature anisotropy. For this calculation, they assumed that the wavevector $\mathbf{k}$ is parallel to the background magnetic field $\mathbf{B_0}$ and took the alpha particles (protons) to have a bi-Maxwellian (Maxwellian) distribution. We note at this point that some authors refer to the parallel FM/W instability as the *parallel FH instability*. Verscharen et al. (2013) validated their analytic results by comparing them to numerical solutions of the hot plasma dispersion relation. For the parameters we consider in this Letter the minimum value of U_α needed to excite the A/IC instability is given by (see Verscharen et al. (2013) for further details)

$$U_\mathrm{A/IC} = v_\mathrm{A} - \sigma\,(R_\alpha - 1)\,w_{\parallel\alpha} - \frac{v_\mathrm{A}^2}{4\sigma\,w_{\parallel\alpha}R_\alpha}, \qquad (1)$$

where $w_{\parallel j} = (2k_B T_{\parallel j}/m_j)^{1/2}$ is the parallel thermal speed and m_j the mass per particle of species j. The minimum value of U_α needed to excite the parallel FM/W instability is

$$U_\mathrm{FM/W} = v_\mathrm{A} - \sigma\,(1 - R_\alpha)\,w_{\parallel\alpha} + \frac{v_\mathrm{A}^2}{4\sigma\,w_{\parallel\alpha}R_\alpha}. \qquad (2)$$

The value of the dimensionless quantity σ in these equations depends very weakly upon the alpha-to-proton density ratio n_α/n_p and the exact definition of the instability threshold. In this Letter, we use the values of σ for which Equations (1) and (2) correspond to growth rates of $10^{-4}\Omega_\mathrm{p}$ (where Ω_p is the proton cyclotron frequency) in a plasma with $n_\alpha/n_\mathrm{p} = 0.05$. These values are $\sigma = 2.4$ in Equation (1) and $\sigma = 2.1$ in Equation (2) (Verscharen et al. 2013). In addition to these approximate analytic instability thresholds, we use numerical solutions of the hot plasma dispersion relation to find contours in different parameter planes (e.g., the $U_\alpha - w_{\parallel\alpha}$ plane) corresponding to various values of the maximum A/IC or FM/W growth rate. To solve the linear dispersion relation we used the following parameters: $n_\alpha/n_\mathrm{p} = 0.05$, $T_\mathrm{e} = T_\mathrm{p}$, $R_\mathrm{p} = 1$, $T_{\parallel\alpha} = 4T_\mathrm{p}$, and $v_A/c = 10^{-4}$, where c is the speed of light. We plot some of these contours in the figures below. As shown by Verscharen et al. (2013), Equations (1) and (2) correspond closely to the numerical contours with $\gamma = 10^{-4}\Omega_\mathrm{p}$, except for the portion of the analytic curve for $U_\mathrm{A/IC}$ at small $w_{\parallel\alpha}/v_\mathrm{A}$ in Figure 1 where $U_\mathrm{A/IC}$ decreases as $w_{\parallel\alpha}/v_\mathrm{A}$ decreases, which is not reproduced in the numerical solutions.

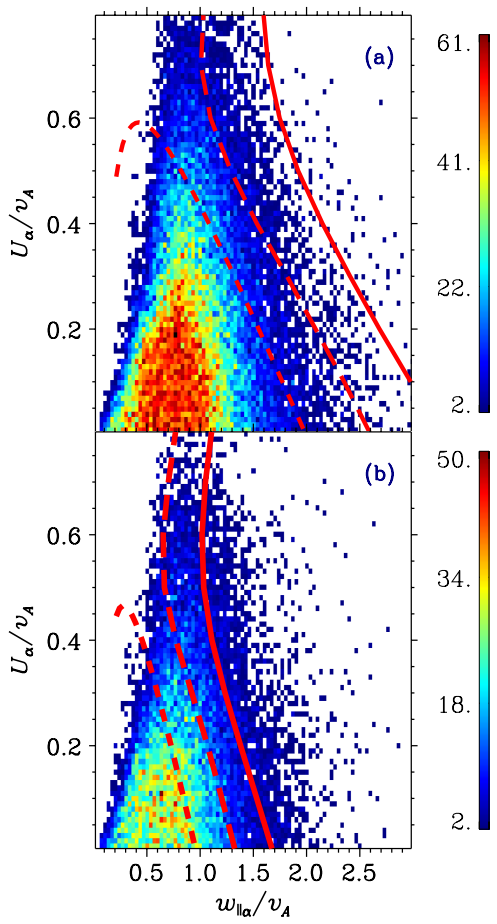

Figure 1. Distribution of data in the $U_\alpha - w_{\parallel\alpha}$ plane, where U_α is the alpha proton drift speed and $w_{\parallel\alpha}$ is the parallel alpha particle thermal speed. The number of measurements in each bin is shown by the color bars on the right. The top panel is the subset of the data in which $1.1 < T_{\perp\alpha}/T_{\parallel\alpha} < 1.3$, and the bottom panel is the subset of the data in which $1.3 < T_{\perp\alpha}/T_{\parallel\alpha} < 1.5$. The short dashed lines are plots of the A/IC instability threshold (Equation (1)) with $T_{\perp\alpha}/T_{\parallel\alpha} = 1.2$ (top panel) and $T_{\perp\alpha}/T_{\parallel\alpha} = 1.4$ (bottom panel). The long dashed (solid) line corresponds to parameter combinations for which the maximum A/IC growth rate is $\gamma = 10^{-3}\Omega_\mathrm{p}$ ($\gamma = 3 \times 10^{-3}\Omega_\mathrm{p}$), where again $T_{\perp\alpha}/T_{\parallel\alpha} = 1.2$ in the top panel and $T_{\perp\alpha}/T_{\parallel\alpha} = 1.4$ in the bottom panel.
(A color version of this figure is available in the online journal.)

In Figure 1, we compare the theoretical instability threshold of the A/IC wave with the subsets of the *Wind* measurements in

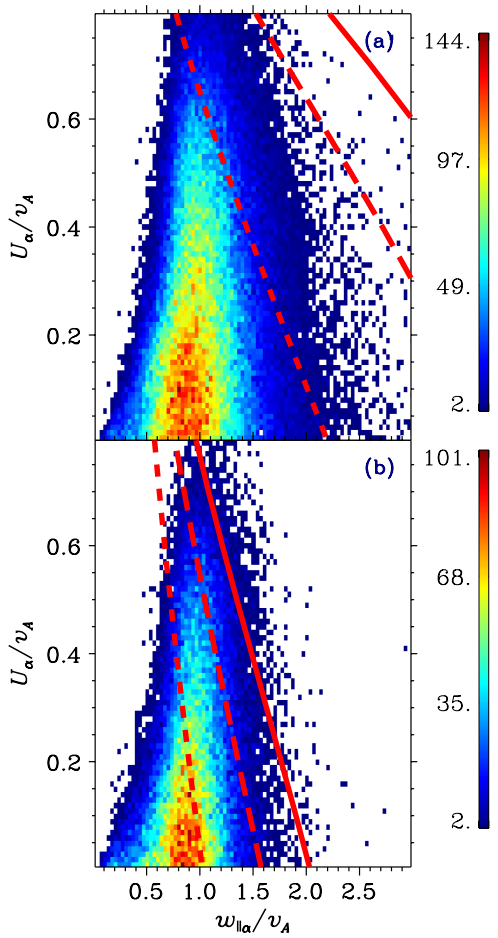

Figure 2. Distribution of data in the $U_\alpha - w_{\|\alpha}$ plane, where U_α is the alpha proton drift speed and $w_{\|\alpha}$ is the parallel alpha particle thermal speed. The number of measurements in each bin is shown by the color bars on the right. The top panel is the subset of the data in which $0.7 < T_{\perp\alpha}/T_{\|\alpha} < 0.9$, and the bottom panel is the subset of the data in which $0.45 < T_{\perp\alpha}/T_{\|\alpha} < 0.55$. The short dashed lines are plots of the FM/W instability threshold (Equation (1)) with $T_{\perp\alpha}/T_{\|\alpha} = 0.8$ (top panel) and $T_{\perp\alpha}/T_{\|\alpha} = 0.5$ (bottom panel). The long dashed (solid) line corresponds to parameter combinations for which the maximum FM/W growth rate is $\gamma = 10^{-3}\Omega_p$ ($\gamma = 3 \times 10^{-3}\Omega_p$), where again $T_{\perp\alpha}/T_{\|\alpha} = 0.8$ in the top panel and $T_{\perp\alpha}/T_{\|\alpha} = 0.5$ in the bottom panel.

(A color version of this figure is available in the online journal.)

which $1.1 < T_{\perp\alpha}/T_{\|\alpha} < 1.3$ (top panel) and $1.3 < T_{\perp\alpha}/T_{\|\alpha} < 1.5$ (bottom panel). We also plot curves corresponding to maximum A/IC growth rates of $10^{-3}\Omega_p$ and $3 \times 10^{-3}\Omega_p$. When $1.1 < T_{\perp\alpha}/T_{\|\alpha} < 1.3$, the large majority of the data is constrained by the analytic threshold in Equation (1), corresponding to a maximum A/IC growth rate of $10^{-4}\Omega_p$. When $1.3 < T_{\perp\alpha}/T_{\|\alpha} < 1.5$, the large majority of the data are constrained to lie below the curve corresponding to a maximum A/IC growth rate of $10^{-3}\Omega_p$. Moreover, the curves corresponding to constant maximum growth rates have approximately the same slope as the contours of the probability distribution function (PDF) of the *Wind* data at $w_{\|\alpha} \gtrsim v_A$.

In Figure 2, we plot the instability threshold of the FM/W wave from Equation (2) along with the subsets of the *Wind* data in which $0.7 < T_{\perp\alpha}/T_{\|\alpha} < 0.9$ (top panel) and $0.45 < T_{\perp\alpha}/T_{\|\alpha} < 0.55$ (bottom panel). We also plot curves corresponding to maximum FM/W growth rates of $10^{-3}\Omega_p$ and $3 \times 10^{-3}\Omega_p$. When $0.7 < T_{\perp\alpha}/T_{\|\alpha} < 0.9$, the majority of the data have values of U_α smaller than the threshold value $U_{FM/W}$ in Equation (2). When $0.45 < T_{\perp\alpha}/T_{\|\alpha} < 0.55$, a small

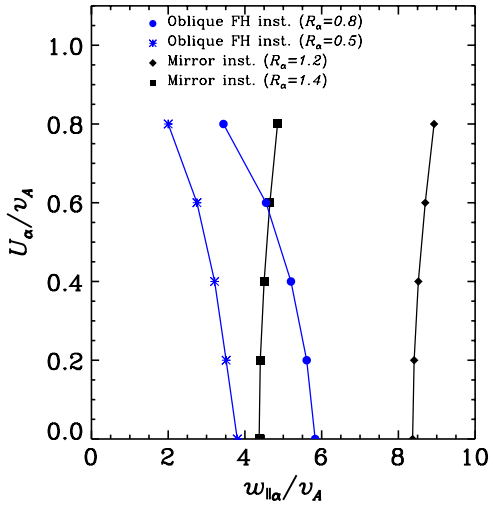

Figure 3. Isocontours of constant maximum growth rate γ for the mirror mode instability with $\gamma = 10^{-3}\Omega_p$ when $R_\alpha = 1.2$ (diamonds) and $R_\alpha = 1.4$ (squares). Isocontours of constant maximum growth rate γ for the oblique FH mode with $\gamma = 10^{-3}\Omega_p$, when $R_\alpha = 0.8$ (filled dots) and $R_\alpha = 0.5$ (asterisks).

(A color version of this figure is available in the online journal.)

fraction of the data satisfies $U_\alpha > U_{FM/W}$, but the majority of the data is constrained to lie below the curve corresponding to $\gamma = 10^{-3}\Omega_p$. In addition, the curves of constant maximum growth rates and the contours of the PDF at $w_{\|\alpha} \gtrsim v_A$ have similar slopes.

We note that the constant-γ contours for the parallel A/IC and FM/W instability thresholds do not coincide with the contours of the data distribution at small $w_{\|\alpha}/v_A$ in Figures 1 and 2, where the upper bound on U_α is approximately proportional to $w_{\|\alpha}$. The reason for this upper bound on U_α at small $w_{\|\alpha}/v_A$ is not clear from our analysis.

Two other instabilities driven by pressure anisotropies are the mirror mode and the oblique FH instabilities (Hellinger & Matsumoto 2002; Pokhotelov et al. 2004; Stix 1992). If the temperature anisotropy crosses the instability threshold of the mirror mode or the oblique FH instability, the unstable mode shows maximum growth rate at a non-vanishing angle between the wavevector k and the background magnetic field B_0. The frequencies of these oblique instabilities in the proton frame are purely imaginary if $U_\alpha = 0$, and the real parts of the frequencies slowly increase with increasing U_α. In Figure 3 we plot numerically determined isocontours of constant maximum growth rates γ for both the mirror mode instability and the oblique FH instability in the $w_{\|}/v_A$-U_α/v_A plane for two different values of R_α. The points represent parameter combinations for which the particular mode has $\gamma = 10^{-3}\Omega_p$ at one wavevector only and has lower γ at all other wavevectors. Both the analytical thresholds and the isocontours with $\gamma = 10^{-3}\Omega_p$ for the A/IC and FM/W instabilities are much closer to the data distribution in parameter space than the isocontours for the oblique instabilities (compare Figure 3 to Figures 1 and 2). Furthermore, the threshold of the mirror mode instability hardly depends on the value of U_α, and the slopes of the lines in Figure 3 are very different from the slopes of the outer contours of the data distribution plotted in Figures 1 and 2. Therefore, we conclude that the oblique instabilities seem not to limit the alpha temperature anisotropy in the presence of alpha drift in our cases.

We now turn to a consideration of the preferential heating of alpha particles near the thresholds of the A/IC and FM/W

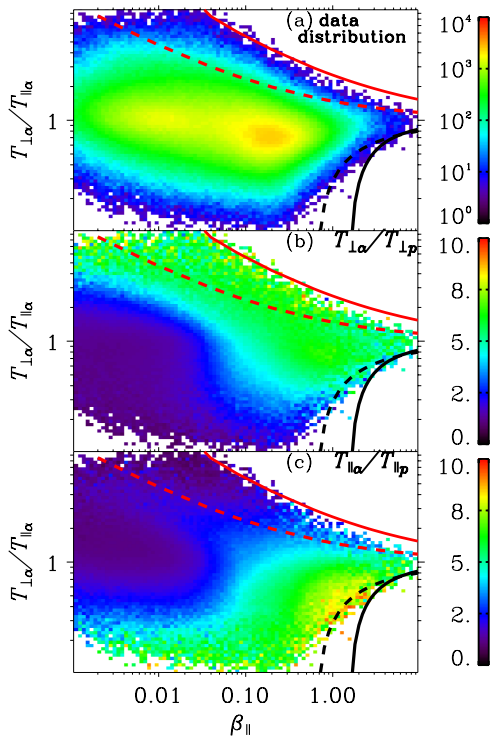

Figure 4. (a) Number of spectra in each bin. Average values of (b) $T_{\perp\alpha}/T_{\perp p}$, and (c) $T_{\parallel\alpha}/T_{\parallel p}$ are given by the color bars on the right. The upper red solid line (red dashed line) represents parameter values for which the maximum growth rate of the mirror mode (A/IC) instability is $\gamma = 10^{-2}\Omega_p$. The lower black solid line (black dashed line) represents parameter values for which the maximum growth rate of the oblique FH (FM/W) instability is $\gamma = 10^{-2}\Omega_p$.

(A color version of this figure is available in the online journal.)

instabilities. For this part of our analysis, we select all data points from the full *Wind* data set between 1994 and mid-2010 for which $U_\alpha < 0.1 v_A$.

In Figure 4 we order the data as a function of $\beta_{\parallel\alpha}$ and $T_{\perp\alpha}/T_{\parallel\alpha}$ (where $\beta_{\parallel\alpha} = 2n_\alpha k_B T_{\parallel\alpha}\mu_0/B_0^2$). The curves in Figure 4 are contours of constant maximum growth rate $\gamma = 10^{-2}\Omega_p$ using the analytical fitting formula (8) of Maruca et al. (2012) assuming isotropic proton temperature, $n_\alpha = 0.05 n_p$ and equal parallel thermal speeds of alpha particles and protons. The curves we plot thus serve primarily to indicate the vicinity of the many different growth rate contours that would apply to this data set. In the top panel of Figure 4, we plot the data distribution as a function of $\beta_{\parallel\alpha}$ and R_α. In the panels (b) and (c) of Figure 4, we plot the average value of $T_{\perp\alpha}/T_{\perp p}$ and $T_{\parallel\alpha}/T_{\parallel p}$, respectively. These plots show that the ratio $T_{\perp\alpha}/T_{\perp p}$ ($T_{\parallel\alpha}/T_{\parallel p}$) is relatively higher near the threshold of the A/IC (FM/W) instability than elsewhere in the ($\beta_{\parallel\alpha}$–$T_{\perp\alpha}/T_{\parallel\alpha}$) plane. This observational finding for alpha particles, to the best of our knowledge, has not been reported before. However, Maruca et al. (2011) reported a similar finding for protons. Although we do not focus on the origin of the enhanced alpha particle temperatures in this study, we note that cyclotron heating and stochastic heating models can explain the preferential heating of alpha particles to temperatures exceeding the proton temperature (Isenberg & Vasquez 2007; Kasper et al. 2013; Chandran et al. 2013).

3. CONCLUSIONS

By analyzing *Wind* measurements of solar wind streams, we find that the alpha particle differential flow is limited to values comparable to the instability thresholds of A/IC and FM/W waves. Importantly, these thresholds depend upon the temperature anisotropy of the alpha particles. In contrast to the U_α thresholds of beam instabilities in isotropic-temperature plasmas, which are $\gtrsim v_A$, the thresholds of the A/IC and FM/W instabilities can be significantly smaller than v_A when $T_{\perp\alpha} \neq T_{\parallel\alpha}$ and when $w_{\parallel\alpha} \gtrsim v_A$. Our findings support previous suggestions that A/IC and FM/W instabilities limit the alpha particle differential flow in the solar wind. Our results also emphasize the importance of treating differential flow and temperature anisotropy on an equal footing when $w_{\parallel\alpha} \gtrsim v_A$, since these properties are of comparable importance for these instabilities.

Within the subset of the data in which $U_\alpha < 0.1 v_A$, we find strong preferential heating of alpha particles relative to protons for conditions under which the A/IC and FM/W instabilities occur. When the plasma is near the threshold of the A/IC instability, $T_{\perp\alpha}/T_{\perp p}$ is unusually large. On the other hand, when the plasma is near the threshold of the FM/W instability, $T_{\parallel\alpha}/T_{\parallel p}$ is unusually large. This suggests that exceptionally strong perpendicular (parallel) heating is the reason why, in a small fraction of the small-U_α data, alpha particles are in the A/IC-unstable (FM/W-unstable) region of parameter space.

We thank Kris Klein for his helpful discussions. This work was supported in part by NASA grants NNX11AJ37G and NNS12AB27G.

REFERENCES

Araneda, J. A., ViñAs, A. F., & Astudillo, H. F. 2002, JGR, 107, 1453
Bale, S. D., Kasper, J. C., Howes, G. G., et al. 2009, PhRvL, 103, 211101
Bourouaine, S., Marsch, E., & Neubauer, F. M. 2008, ApJL, 684, L119
Bourouaine, S., Marsch, E., & Neubauer, F. M. 2010, GeoRL, 37, 14104
Bourouaine, S., Marsch, E., & Neubauer, F. M. 2011a, ApJL, 728, L3
Bourouaine, S., Marsch, E., & Neubauer, F. M. 2011b, A&A, 536, A39
Chandran, B. D. G., Li, B., Rogers, B. N., Quataert, E., & Germaschewski, K. 2010, ApJ, 720, 503
Chandran, B. D. G., Verscharen, D., Quataert, E., et al. 2013, ApJ, 776, 45
Chew, G. F., Goldberger, M. L., & Low, F. E. 1956, RSPSA, 236, 112
Dmitruk, P., Matthaeus, W. H., & Seenu, N. 2004, ApJ, 617, 667
Gary, S. P. 1993, Theory of Space Plasma Microinstabilities (Cambridge: Cambridge Univ. Press)
Gary, S. P., Yin, L., & Winske, D. 2006, JGR, 111, 6105
Gary, S. P., Yin, L., Winske, D., Ofman, L., Goldstein, B. E., & Neugebauer, M. 2003, JGR, 108, 1068
Gary, S. P., Yin, L., Winske, D., & Reisenfeld, D. B. 2000, GeoRL, 27, 1355
Hellinger, P., & Matsumoto, H. 2002, JGR, 105, 10519
Hellinger, P., Trávníček, P., Kasper, J. C., & Lazarus, A. J. 2006, GeoRL, 33, 9101
Hellinger, P., Trávníček, P., Mangeney, A., & Grappin, R. 2003, GeoRL, 30, 1959
Hollweg, J. V., & Isenberg, P. A. 2002, JGR, 107, 1147
Isenberg, P. A., Lee, M. A., & Hollweg, J. V. 2001, JGR, 106, 5649
Isenberg, P. A., & Vasquez, B. J. 2007, ApJ, 668, 546
Kaghashvili, E. K., Vasquez, B. J., Zank, G. P., & Hollweg, J. V. 2004, JGR, 109, 12101
Kasper, J. C. 2002, PhD thesis, Massachusetts Institute of Technology
Kasper, J. C., Lazarus, A. J., & Gary, S. P. 2002, GeoRL, 29, 1839
Kasper, J. C., Lazarus, A. J., & Gary, S. P. 2008, PhRvL, 101, 261103
Kasper, J. C., Lazarus, A. J., Steinberg, J. T., Ogilvie, K. W., & Szabo, A. 2006, JGR, 111, 3105
Kasper, J. C., Maruca, B. A., Stevens, M. L., & Zaslavsky, A. 2013, PhRvL, 110, 091102
Kennel, C. F., & Wong, H. V. 1967, JPlPh, 1, 75
Lepping, R. P., Acũna, M. H., Burlaga, L. F., et al. 1995, SSRv, 71, 207
Li, X., & Habbal, S. R. 2000, JGR, 105, 7483
Lu, Q., Du, A., & Li, X. 2009, PhPl, 16, 042901
Marsch, E. 2006, LRSP, 3, 1

Marsch, E., Schwenn, R., Rosenbauer, H., Muehlhaeuser, K.-H., Pilipp, W., & Neubauer, F. M. 1982, JGR, 87, 52
Marsch, E., & Tu, C.-Y. 2001, JGR, 106, 227
Maruca, B. A. 2012, PhD thesis, Harvard Univ.
Maruca, B. A., & Kasper, J. C. 2013, AdSpR, 52, 723
Maruca, B. A., Kasper, J. C., & Bale, S. D. 2011, PhRvL, 107, 201101
Maruca, B. A., Kasper, J. C., & Gary, S. P. 2012, ApJ, 748, 137
Neugebauer, M., Goldstein, B. E., Bame, S. J., & Feldman, W. C. 1994, JGR, 99, 2505
Ogilvie, K. W., Chornay, D. J., Fritzenreiter, R. J., et al. 1995, SSRv, 71, 55
Parashar, T. N., Shay, M. A., Cassak, P. A., & Matthaeus, W. H. 2009, PhPl, 16, 032310
Pokhotelov, O. A., Sagdeev, R. Z., Balikhin, M. A., & Treumann, R. A. 2004, JGR, 109, 9213
Stix, T. H. 1992, Waves in Plasmas (New York: AIP)
Verscharen, D., Bourouaine, S., & Chandran, B. D. G. 2013, ApJ, 773, 163
Verscharen, D., & Chandran, B. D. G. 2013, ApJ, 764, 88